



HAL
open science

Cholinergic modulation inhibits cortical spreading depression in mouse neocortex through activation of muscarinic receptors and decreased excitatory/inhibitory drive

Sarah Zerimech, Oana Chever, Paolo Scalmani, Lara Pizzamiglio, Fabrice Duprat, Massimo Mantegazza

► To cite this version:

Sarah Zerimech, Oana Chever, Paolo Scalmani, Lara Pizzamiglio, Fabrice Duprat, et al.. Cholinergic modulation inhibits cortical spreading depression in mouse neocortex through activation of muscarinic receptors and decreased excitatory/inhibitory drive. *Neuropharmacology*, 2020, 166, pp.107951. 10.1016/j.neuropharm.2020.107951 . hal-02454613

HAL Id: hal-02454613

<https://hal.science/hal-02454613>

Submitted on 24 Jan 2020

HAL is a multi-disciplinary open access archive for the deposit and dissemination of scientific research documents, whether they are published or not. The documents may come from teaching and research institutions in France or abroad, or from public or private research centers.

L'archive ouverte pluridisciplinaire **HAL**, est destinée au dépôt et à la diffusion de documents scientifiques de niveau recherche, publiés ou non, émanant des établissements d'enseignement et de recherche français ou étrangers, des laboratoires publics ou privés.

Cholinergic modulation inhibits cortical spreading depression in mouse neocortex through activation of muscarinic receptors and decreased excitatory/inhibitory drive.

Neuropharmacology. 2020 Jan 13;166:107951.

doi: 10.1016/j.neuropharm.2020.107951.

PMID: 31945385

Sarah Zerimech^{1,2}, Oana Chever^{1,2, a}, Paolo Scalmani³, Lara Pizzamiglio^{1,2}, Fabrice Duprat^{1,2,4},

Massimo Mantegazza^{1,2,4, #}

1 Université Côte d'Azur, Valbonne-Sophia Antipolis, France.

2 CNRS UMR7275, Institute of Molecular and Cellular Pharmacology (IPMC), Valbonne-Sophia Antipolis, France.

3 U.O. Neurophysiopathology and Diagnostic Epileptology, Foundation IRCCS Neurological Institute Carlo Besta, Milan, Italy.

4 Inserm, Valbonne-Sophia Antipolis, France.

Corresponding Author: Massimo Mantegazza: mantegazza@ipmc.cnrs.fr

Institute of Molecular and Cellular Pharmacology (IPMC), CNRS UMR 7275 and Université Côte d'Azur, 660 Route des Lucioles, 06560 Valbonne-Sophia Antipolis, France. Tel. +33 (0)493953425 FAX +33 (0)493957708

a Present address: Normandie University, UNIROUEN, INSERM U1239, DC2N, 76000 Rouen, France.

Running title: Muscarinic modulation inhibits CSD.

Keywords: migraine, aura, spreading depolarization, acetylcholine, UP-DOWN states, carbachol, excitation, inhibition.

Abstract

Cortical spreading depression (CSD) is a wave of transient network hyperexcitability leading to long lasting depolarization and block of firing, which initiates focally and slowly propagates in the cerebral cortex. It causes migraine aura and it has been implicated in the generation of migraine headache. Cortical excitability can be modulated by cholinergic actions, leading in neocortical slices to the generation of rhythmic synchronous activities (UP/DOWN states).

We investigated the effect of cholinergic activation with the cholinomimetic agonist carbachol on CSD triggered with 130mM KCl pulse injections in acute mouse neocortical brain slices, hypothesizing that the cholinergic-induced increase of cortical network excitability during UP states could facilitate CSD. We observed instead an inhibitory effect of cholinergic activation on both initiation and propagation of CSD, through the action of muscarinic receptors. In fact, carbachol-induced CSD inhibition was blocked by atropine or by the preferential M1 muscarinic antagonist telenzepine; the preferential M1 muscarinic agonist McN-A-343 inhibited CSD similarly to carbachol, and its effect was blocked by telenzepine. Recordings of spontaneous excitatory and inhibitory post-synaptic currents in pyramidal neurons showed that McN-A-343 induced overall a decrease of the excitatory/inhibitory ratio. This inhibitory action may be targeted for novel pharmacological approaches in the treatment of migraine with muscarinic agonists.

1. Introduction

Cortical spreading depression (CSD) is a wave of transient intense network hyperexcitability leading to a long lasting depolarization and block of neuronal firing, which initiates focally and slowly propagates in the cerebral cortex in normoxic conditions (Ayata and Lauritzen, 2015; Dreier and Reiffurth, 2015). CSD has been causally related to migraine aura and proposed to be the trigger of neurogenic inflammation, leading to sensitization of meningeal nociceptors and migraine headache (Karatas et al., 2013; Lauritzen, 1994; Pietrobon and Moskowitz, 2013). Moreover, spreading depolarizations that show some similarities to CSD can be induced by ischemic/hypoxic conditions, facilitating neuronal death, and can propagate from an energy-depleted tissue into surrounding normoxic tissue, as it is often observed in stroke and brain trauma (Dreier and Reiffurth, 2015). Mechanisms of CSD initiation and propagation, which are characterized by different features and mechanisms, are not completely understood yet, although increased extracellular K^+ concentration and increased release of the excitatory neurotransmitter glutamate are important factors (Pietrobon and Moskowitz, 2014). Thus, migraine is a complex disorder, in which altered excitation-inhibition balance and hyperexcitability of cortical networks can be important pathological mechanisms (Pietrobon and Moskowitz, 2014; Vinogradova, 2018). Notably, they can have similarities with those that trigger epileptic seizures, although the exact differential mechanisms and the relationships between CSD and epileptic activity are not completely understood (Mantegazza and Cestele, 2018).

Cortical excitability is influenced by numerous neuromodulators. In particular, acetylcholine plays a major role in cortical arousal and desynchronization typical of awakening and REM sleep (Munoz and Rudy, 2014; Poorthuis et al., 2014), but basal cholinergic tone is also essential for the generation of slow rhythmic oscillations, UP/DOWN states, which are typical

of slow-wave sleep and anesthesia, and are generated by cortical pyramidal neurons (Beltramo et al., 2013; Lorincz et al., 2015). Acetylcholine acts on both ionotropic nicotinic receptors and metabotropic muscarinic receptors. Its effect on the excitability of cortical neurons is complex, depending of the subtype of neuron and the subtype of receptor (Munoz and Rudy, 2014), but a prominent overall effect of cholinergic inputs is the disinhibition and depolarization of excitatory pyramidal neurons (Kurowski et al., 2015; Lorincz et al., 2015; Poorthuis et al., 2014; Wester and Contreras, 2013).

Carbachol is a broad spectrum cholinomimetic agonist that activates both muscarinic and nicotinic receptors; it is often used to induce cholinergic activation in cortical and hippocampal slices, “disconnected” preparations in which it can induce rhythmic activities, for example UP/DOWN states in neocortical slices (Lorincz et al., 2015). Migraine-related studies have shown that blood infusion of carbachol can induce dilation of cephalic arteries and subsequent headache, but not migraine attacks (Schytz et al., 2010; Schytz et al., 2009). Notably, it has been shown that the non-specific muscarinic agonist pilocarpine at subconvulsive doses can decelerate CSD in anesthetized rats (Francisco and Guedes, 2018). However, the effect of central cholinergic modulation on migraine pathological mechanisms and its use in therapeutic interventions against spreading depolarizations has not been thoroughly investigated (Klass et al., 2018).

We studied here the role of cholinergic activation on CSD triggered with KCl injections in acute mouse neocortical brain slices, hypothesizing that the cholinergic-induced increase of cortical networks’ excitability during UP states could facilitate CSD. Interestingly, we observed an inhibitory effect of cholinergic activation by carbachol through the action of muscarinic receptors, probably preponderantly of the M1 subtype, which may be a target in migraine therapy.

2. Material and methods.

2.1 Animal care and mouse lines.

Experiments were carried out with C57BL/6J mice (Charles River, France and Italy) according to the European directive 2010/63/UE and approved by institutional and ethical committees (approval #C06-152-5 for France, 711/2016-PR for Italy). All efforts were made to minimize the number of animals used and their suffering. Animals were group housed (5 mice per cage, or 1 male and 2 females per cage for breeding) on a 12h light/dark cycle, with water and food ad libitum.

2.2 Preparation of slices.

Brain slices were prepared from 25-40 day-old mice of both sexes as previously described (Hedrich et al., 2014; Liautard et al., 2013). Briefly, mice were killed by decapitation under isoflurane anesthesia, the brain was quickly removed and placed in ice-cold artificial cerebrospinal fluid (ACSF), which contained (in mM): 125 NaCl, 2.5 KCl, 2 CaCl₂, 1 MgCl₂, 1.25 NaH₂PO₄, 25 NaHCO₃ and 25 glucose, saturated with 95 % O₂ - 5 % CO₂. Acute coronal slices (400 µm thick for field potential and imaging experiments, 300 µm thick for patch-clamp experiments) were prepared with a vibratome (HM650V, MicroM or Leica VT1200S, Germany) in ice-cold ACSF. Slices were then stored in a submerged chamber with ACSF at 32°C at least one hour before the beginning of the recordings.

2.3 Electrophysiological recordings and CSD quantification by intrinsic optical signal analysis

Single slices were placed in a submerged recording chamber (Warner Instr., USA) mounted on an Eclipse FN1 microscope (Nikon, Japan) and perfused with a modified ACSF solution (mACSF;

3-4 ml/min), which was heated at 32°C and saturated with 95% O₂-5% CO₂. The mACSF contained (in mM): 125 NaCl, 3.5 KCl, 1 CaCl₂, 0.5 MgCl₂, 1.25 NaH₂PO₄, 25 NaHCO₃ and 25 glucose (Tottene et al., 2009).

Cortical spreading depression was induced by brief pulses of KCl 130 mM applied in superficial layers (L2-3) of the somatosensory cortex with a glass micropipette (2-4 MΩ) connected to an air pressure injector (holding pressure: < 1 PSI, injection pressure: 7 to 10 PSI; PV820 Pneumatic Picopump, WPI, USA). Fastgreen (0.1 %, SIGMA-Aldrich, USA) was added to the pipette solutions to quantify the injection area, which was measured with ImageJ-Fiji (Schindelin et al., 2015) by drawing the limits of the dark zone observed in the slice at the end of the injection and obtaining the value of the enclosed area. This is a more reliable measurement than the picopump injected volume, because it is a quantification of the actual volume injected into the tissue, which does not include the volume leaked into the perfusing solution that in some experiments can be considerable (for example, see Supplementary Video 2). The area of injection was increased by repeating the injections (inter-injection interval 1 min) until CSD was ignited, which defined the CSD threshold. A single CSD was induced in each slice. Applications of control 0.9% NaCl solutions with Fastgreen never ignited CSD.

Intrinsic optical signal (IOS: near-infrared light transmittance) (Holthoff and Witte, 1996) was monitored acquiring images with a CoolSnap ES2 CCD camera controlled with micromanager (Edelstein et al., 2014) at 1 image/s. Image analysis was used to identify the CSD wave front using ImageJ-Fiji. Image processing with a custom made ImageJ-Fiji macro (csd_analysis, available at <https://www.ipmc.cnrs.fr/~duprat/scripts/imagej.htm>) was used to quantify CSD threshold and propagation speed: to eliminate the background and isolate the wave from the raw image, a representative image acquired before the KCl injection was subtracted from the

others and then white and black contrast was enhanced. To determine the velocity of the propagating wave, successive line plots of the wave front from processed images (every 2 seconds) were drawn, and the spatial distances between them were quantified by means of the peak finder ImageJ plugin. For each slice, speed was estimated on a minimum of 4 time points (a total of 8 s).

Electrophysiological experiments were performed using borosilicate glass micropipettes, Multiclamp 700B amplifier, Digidata 1440A acquisition board and pClamp 10.3 software (Molecular Devices, USA). For extracellular DC local field potential recordings, pipettes were filled with mACSF (0.5-1 M Ω) and placed about 500 μ m away from the CSD site of induction; LFP were not recorded in all the experiments (the “n” of LFP recordings can be different compared with the “n” of IOS acquisitions). Spontaneous postsynaptic currents were measured by means of whole-cell patch-clamp recordings obtained from pyramidal neurons in layer 2-3 of the somatosensory neocortex. The patch-clamp electrodes (3-5 M Ω) were filled with the following solution (in mM): 120 K-gluconate, 15 KCl; 0.2 EGTA, 2 MgCl₂, 10 HEPES, 2 Na₂-ATP, 0.2 Na₂-GTP, 20 phosphocreatine di(tris), pH was adjusted to 7.2 with KOH. Recordings of spontaneous excitatory postsynaptic currents (sEPSCs) were performed at -60 mV, whereas spontaneous inhibitory postsynaptic currents (sIPSCs) were recorded at +10 mV. In fact, -60 mV was the reversal potential of sIPSCs measured in preliminary experiments in the presence of the glutamate receptor blocker kynurenic acid (1 mM) and +10 mV the reversal potential of sEPSCs measured in the presence of the GABA-A receptor blocker gabazine (15 μ M). Pyramidal neurons were identified by their morphology (using infrared differential interference contrast, DIC, microscopy) and by their firing pattern obtained with injections of depolarizing current steps in current-clamp before to record post synaptic currents (firing patterns were of the regular spiking type; not shown). Postsynaptic current

properties were quantified on a 103 s time window; the total charge transferred was calculated integrating the postsynaptic current events.

Signals were filtered at 10 kHz and sampled at 25 kHz. Analyses were performed on offline filtered traces (1kHz for LFP, 500 Hz for post synaptic currents) using pClamp 10.3.

2.4 Pharmacology

For each day of experiment, CSD were induced both in control slices and in slices treated with the drug(s) under study (100 μ M carbachol, or 100 μ M carbachol + 10 μ M atropine, or 10 μ M atropine, or 100 μ M carbachol + 100 nM telenzepine, or 30 μ M McN-A-34, or 30 μ M McN-A-34 + 100 nM telenzepine). Carbachol (carbamoylcholine chloride), atropine (atropine sulfate salt monohydrate), kynurenic acid and gabazine were bought from Sigma-Aldrich (USA), McN-A-343 and telenzepine dihydrochloride from Tocris Bioscience (UK). Salts were bought from Sigma-Aldrich (USA).

2.5 Statistical analysis

The reported “n” is the number of slices used for each condition; each experiment was performed using at least 3 animals. Statistical tests were performed with Prism 5 (GraphPad, USA) or Origin 8 (Origin Lab. Corp, USA). We used the two-tailed non parametric Mann-Whitney U test (for comparing two unpaired groups), the Wilcoxon matched-pairs test (for comparing two paired groups), the Kruskal-Wallis test with the Dunn’s post-hoc test (for comparing more than two groups), the Fischer’s exact test (for comparing proportions), the Kolgomorov-Smirnof (K-S) test for comparing cumulative probability curves and the t-test for comparing the normally distributed mean values of post synaptic current properties.

Differences were considered significant at $p < 0.05$. In the figures, * is $p < 0.05$, ** is $p < 0.01$, *** is $p < 0.001$ and **** is $p < 0.0001$.

3. Results

CSD can be induced in brain tissue both *in vitro* and *in vivo* by applications of KCl at high concentration (Pietrobon and Moskowitz, 2014). Often, very high concentrations of KCl have been used, up to 2M, which are far above pathophysiological limits. We triggered CSD by injecting brief pulses (puffs) of 130 mM KCl into the superficial layers of somatosensory cortex mouse brain slices (Fig.1A), concentration that is within pathophysiological limits and can better disclose real pathophysiological properties of CSD, in particular those related to initiation (Tang et al., 2014). We initially characterized the properties of CSD in our control experimental conditions, simultaneously monitoring CSD by electrophysiological local field potential (LFP) recordings and intrinsic optical signal (IOS) imaging (Holthoff and Witte, 1996). LFP recordings showed the typical profile observed during CSD, with a DC shift composed by a faster negative peak phase and a slower later phase with return at the baseline (Fig.1B, upper right panel). We used IOS imaging to quantify CSD propagation properties in the neocortex (Fig.1B, lower panels, and Supplementary Video 1). It has been reported that spreading depolarizations shows layer-specific features, propagating preferentially along the upper layers of the neocortex (Basarsky et al., 1998; Leao, 1947). Thus, we measured the propagation speed both along the superficial layers and to the deep layers, confirming that propagation to deep layers (L4-6) was 31% slower than along superficial layers (L1-3) (Fig.1D). Thus, in subsequent experiments we evaluated modifications of the speed of propagation both along superficial layers and to deep layers.

To study the effect of tonic activation of cholinergic receptors on CSD properties, we pre-incubated brain slices with mACSF and 100 μ M carbachol in a holding chamber for 30 minutes at 32°C. Then the slices were transferred into the recording chamber and perfused with mACSF and 100 μ M carbachol at 32°C.

We initially evaluated the effect of carbachol on the excitability of the cortical network, performing LFP recordings simultaneously in layers 3 and 5 of the somatosensory cortex from the same hemisphere. The application of carbachol induced rhythmic oscillatory activities (UP/DOWN states) that were particularly evident in the layer 5 and much less in superficial layers (Fig.2A), as it has been previously described (Lorincz et al., 2015). Thus, also in our preparation the pharmacological activation of cholinergic receptors can generate periods of enhanced cortical excitability.

We ignited CSD by puff injections of 130mM KCl in layer 2-3 both in control and in the presence of carbachol. The LFP correlate of CSD was similar in the two conditions, characterized by a biphasic DC shift whose amplitude and duration were not modified by carbachol (Fig.2B). However, with carbachol the threshold of CSD ignition (minimal area of KCl injection) was increased by 1.92 fold compared to control values, consistent with an inhibition of CSD initiation (Fig.2C). Carbachol also induced a decrease of CSD propagation speed in both superficial (31% decrease) and deep (56% decrease) layers compared to the control condition (Fig.2D). Moreover, in the presence of carbachol, we observed that some CSDs could be self-limited, because they were induced by the puff of KCl and initially had properties (threshold and propagation speeds) that were similar to standard CSDs (Fig.2C & D), but stopped before to propagate in the whole cortical tissue. Fig.3A and Supplementary Video 2 show one of these abortive CSD with propagation limited to a few hundred μm around the pipette used to inject KCl and that did not reach Layer 1 and the pial surface. Overall, abortive CSD were observed in 14% of the slices treated with carbachol and never in control conditions ($p=0.037$, Fisher's exact test) (Fig.3B). We were able to record in two experiments the LFP around the limit of CSD propagation (e.g. Fig.3A); it appeared smaller and shorter (peak amplitude 1.1 ± 0.3 mV,

half-width 6.4 ± 0.4 s) than that recorded from control, non-abortive CSD or at the beginning of the propagation of abortive CSD.

Thus, these results are consistent with the inhibition of both induction and propagation of CSD by cholinergic activation, although cholinergic activation can increase cortical excitability during UP states.

Carbachol is a cholinomimetic agent that can activate both muscarinic and nicotinic acetylcholine receptors. To find out which pathway is involved in CSD inhibition, we used atropine, an antagonist of muscarinic receptors, and, telenzepine, a M1 receptor-preferring antagonists (Fig.4), because the M1 receptor is the predominant muscarinic receptor expressed in the neocortex (Lebois et al., 2018). Telenzepine has been used at the concentration of 100 nM in several studies for investigating selective M1 actions in neurons, for example: (Li et al., 2009; Williams and Fletcher, 2019). All slices were pre-incubated with mACSF and carbachol 100 μ M, carbachol 100 μ M and atropine 10 μ M, atropine 10 μ M alone or carbachol 100 μ M and telenzepine 100 nM; then, they were transferred into the recording chamber and perfused with the corresponding drugs. Experiments in which atropine was applied together with carbachol showed that the muscarinic antagonist blocked the inhibitory effect of carbachol on both induction and propagation of CSD. In fact, injection area and propagation speed in both superficial and deep layers reverted to control values. Atropine alone did not modify CSD properties compared to the control condition. Application of telenzepine with carbachol reverted the effect of carbachol to control values, similarly to the results obtained applying atropine with carbachol.

Therefore, the inhibition of CSD by carbachol is induced by the activation of muscarinic receptors, probably through the M1 subtype.

We then investigated if activation of M1 muscarinic receptors could have effects that are similar to those observed with carbachol. We used McN-A-343 at the concentration of 30 μ M, a muscarinic agonist with in general a preponderant effect on the M1 muscarinic receptor subtype (Mitchelson, 2012). Before to trigger CSD, we performed LFP recordings simultaneously in layers 3 and 5 of the neocortex from the same hemisphere. Differently than carbachol, McN-A-343 did not induce rhythmic UP/DOWN states, and we did not observe any obvious modifications of activity in comparison with the control condition. Puff injections of 130mM KCl induced CSD both in control and with McN-A-343 (Fig. 5). Peak amplitude and duration of the DC shift observed in LFP recordings were similar in the two conditions (Fig.5A legend). However, with McN-A-343, the threshold of induction showed a 2.7-fold increase (Fig.5B) and the speed of propagation was reduced by 36% in superficial layers (Fig.5C, left). In deep layers the speed of propagation showed a non-statistically significant trend towards reduction (Fig.5C, right). Similar to carbachol, 18% of the CSDs induced in the presence of McN-A-343 were abortive, showing a self-limited propagation ($632\pm 116\mu\text{m}$ along the superficial layers) that was never observed in control (Fisher's exact test, $p=0.037$). Their threshold of induction was similar to that of the other CSD events observed with McN-A-343, although the initial propagation speed was among the lower ones in the McN-A-343 (Fig.5B, C). Additionally, to investigate if the effect was mediated by M1 receptors, we tested the action of telenzepine on the McN-A-343-induced CSD inhibition. When McN-A-343 (30 μ M) was applied with telenzepine (100nM), neither threshold of CSD induction nor its propagation speed in superficial or deep layers were modified in comparison with the control condition (Fig.5D,E). Moreover, we never observed aborted CSDs with application of McN-A-343 and telenzepine.

Further, we studied the mechanism of CSD inhibition induced by muscarinic receptor activation. We evaluated the effect of McN-A-343 (30 μ M) on spontaneous excitatory postsynaptic currents (sEPSCs) recorded at -60mV and spontaneous inhibitory

postsynaptic currents (sIPSCs) recorded at +10mV from pyramidal neurons of layer 2-3, without using any blockers of glutamatergic or GABAergic receptors (Fig 6). These experiments provide a measure of the excitatory and inhibitory drive experienced by pyramidal neurons. With McN-A-343, we observed a reduction of the frequency of sEPSCs (20% on average; Fig. 6B), consistent with a reduced excitatory drive, but also an increase of their peak amplitude (34% Fig 6C), which is consistent with increased excitatory drive. To evaluate the overall effect, we calculated the total charge transferred by the sEPSCs during a 103s time window, observing on average a 40% reduction. Thus, McN-A-343 had differential effects on frequency and peak amplitude of sEPSCs, but the overall effect was a reduction of the excitatory drive. Analysis of sIPSCs revealed a strong increase of the frequency of the events (150%; Fig. 6F) and a more moderate increase of their amplitude (30%; Fig. 6G), leading to a large increase of the charge transferred by sIPSCs (305%; Fig. 6H). Thus, McN-A-343 induced a net overall increase of the inhibitory drive and a decrease of the excitatory drive, leading to a shift of the excitatory/inhibitory balance towards reduced excitability.

Altogether, these results demonstrate that cholinergic activity, through muscarinic receptors (particularly of the M1 subtype), inhibits both initiation and propagation of CSD in the mouse neocortex, mainly by decreasing the excitatory/inhibitory drive in pyramidal neurons.

4. Discussion

Hyperexcitability leading to synchronous neuronal activity is observed in the initial phase of CSD and is implicated in its generation (Mantegazza and Cestele, 2018; Pietrobon and Moskowitz, 2014; Vinogradova, 2018). Rhythmic activities characterized by periods of neuronal depolarization and increased synchronous excitability are observed in hippocampal and cortical brain slices, and are similar to slow oscillations observed *in vivo* during slow sleep and certain types of anesthesia. In the neocortex, they are called UP/DOWN states, in which the UP state is generated by the activity of pyramidal neurons in Layer 5 and propagates through the neocortex (Beltramo et al., 2013; Lorincz et al., 2015; Sanchez-Vives and McCormick, 2000).

Cholinergic activation, in general obtained in brain slices with application of carbachol, can depolarize pyramidal neurons, engage them and sustain the generation of UP states (Lorincz et al., 2015; Wester and Contreras, 2013). We confirmed in our preparation that carbachol induced rhythmic UP states in the neocortex, which in LFP recordings are larger and more easily identifiable in layer 5 than in other layers. However, this pro-excitatory action of carbachol did not facilitate CSD. On the contrary, we observed that CSD was inhibited by the cholinergic activation and we showed that this inhibitory action is carried out by muscarinic receptors, probably in particular of the M1 subtype, which is the most expressed muscarinic subtype in the neocortex (Lebois et al., 2018). In fact, 1) the muscarinic antagonist atropine blocked the inhibitory effect of carbachol on CSD, 2) the effects on CSD of the preferential M1 muscarinic receptor agonist McN-A-343 were similar to those observed with carbachol, and 3) the preferential M1 receptor antagonist telenzepine blocked the effect of both carbachol and McN-A-343. Thus, in our experiments, we demonstrate that CSD inhibition was not related to the cholinergic induction of increased excitability during UP states

Cholinergic actions are characterized by numerous mechanisms that activate different pathways, and other modulations may counteract the putative facilitating effect possibly played by the network activation on CSD during UP states. Consistently, the application of McN-A-343 inhibited CSD, but in this condition we did not observe the UP states that were evident with carbachol. Our investigation of the modifications induced by McN-A-343 on the synaptic drive of pyramidal neurons, showed that there was an overall decrease of the excitatory/inhibitory ratio. Notably, this result contrast with previous reports that used the non-selective muscarinic agonist pilocarpine, in which it has been proposed that a shift of the excitatory/inhibitory balance towards hyperexcitability can inhibit, rather than facilitate, CSD. In particular, CSD was inhibited in chronic epileptic rats generated by status epilepticus induced with systemic injections of pilocarpine, effect that was reverted by increasing GABA-A activity with diazepam (Guedes and Cavalheiro, 1997), and treatment with sub-convulsive doses of pilocarpine reduced CSD propagation velocity in anesthetized naïve rats (Francisco and Guedes, 2018). Similarly, it has been shown that CSD does not penetrate into penicillin-generated cortical epileptic foci or electrically stimulated (6-10Hz) cortical areas of anesthetized rats (Koroleva and Bures, 1979). However, in our experiments, CSD was inhibited by muscarinic pathways independently of the cholinergic-mediated induction of UP/DOWN states. The experimental system in these studies was different in comparison with our study (anesthetized rats vs acute mouse brain slices). However, we could speculate that possible causes of the discrepancies might be linked to differential activation of muscarinic receptor subtypes and cell-specific biased signaling obtained with different cholinergic agonists; for instance, pilocarpine shows more pronounced selectivity for the M3 vs M1 receptors in comparison with McN-A-343 (Mitchelson, 2012; Pronin et al., 2017). Additionally, this could be coupled to different modifications of excitability, with more sustained and profound

hyperexcitability that could induce remodeling of neuronal circuits, leading, for example, to increased extracellular K⁺ buffering that would inhibit CSD (Guedes and Cavalheiro, 1997; Koroleva and Bures, 1980).

Inhibitory muscarinic actions that could be consistent with CSD inhibition and decreased excitatory/inhibitory ratio have been reported. For example, *in vivo* microinjections in the rat anterior cingulate cortex of McN-A-343 (the same preferential M1 agonist that we have used) induced increased GABAergic synaptic transmission and anti-nociceptive effects to mechanical stimuli (Koga et al., 2017). Moreover, muscarinic actions have been implicated in long term depression (LTD) of synaptic functions. LTD facilitation induced by carbachol application has been reported in rat visual cortex slices, which was mediated by the activation of muscarinic receptors, probably M1, and was NMDA receptor-dependent (Kirkwood et al., 1999). In the CA1 area of rat hippocampal slices, stimulation of cholinergic receptors with carbachol or the M1 preferential agonist 77-LH-28-1 induced LTD (muscarinic LTD or mLTD), which was prevented by the muscarinic antagonist pirenzepine, was NMDA receptor-dependent, and was linked to NMDA receptors internalization (Jo et al., 2010). Activation of M1 muscarinic receptors induce mLTD also in the prefrontal cortex, where it could depend on the co-activation of mGluR5 glutamate receptors, and also lead to increased GABAergic transmission on pyramidal neurons (Ghoshal et al., 2017). LTD of glutamatergic synaptic transmission, which often leads to reduction of functional NMDA receptors, could be involved in CSD inhibition. In fact, propagation of CSD induced by focal KCl application is inhibited by the block of NMDA receptor, although the involvement of NMDA receptors in CSD induction is controversial (Pietrobon and Moskowitz, 2014). In line with the complexity of muscarinic actions, there are also reports of increased neuronal excitability upon muscarinic activation, which are not consistent with the decreased excitatory/inhibitory ratio that we have

observed, but may be consistent with the increased amplitude of sEPSCs that we found. For instance, muscarinic receptor agonists induced membrane potential depolarization through the M1 receptor-dependent activation of sodium channels in rat medial prefrontal cortex pyramidal neurons (Kurowski et al., 2015), and M1 activation increased intrinsic neuronal excitability in the CA1 area of the hippocampus (Thorn et al., 2017).

Notably, anesthetics can induce *in vivo* slow rhythmic activity, including cortical UP/DOWN states, and some of them can inhibit CSD, although there are controversial reports about their effect on CSD (Klass et al., 2018). Similar to cholinergic modulations, anesthetics show complex mechanisms and some of them can reduce neuronal network excitability in the neocortex (Becker et al., 2012; Voss et al., 2019).

Interestingly, both initiation and propagation of CSD were inhibited in our experiments, although they are characterized by different mechanisms (Pietrobon and Moskowitz, 2014). In particular, in some experiments, CSD propagation was blocked and it did not reach the pial surface of the slice; *in vivo*, this could prevent the sensitization of meningeal nociceptors that has been proposed to be involved in headache generation (Karatas et al., 2013). Thus, the muscarinic modulation can induce both an increase of the threshold of CSD ignition and an inhibition of its propagation. In some cases, we observed that this can lead to self-limited abortive CSD. These are synergic effects that could be used in migraine therapy for inhibiting CSD and its consequences, and possibly in other pathological conditions in which spreading depolarizations are involved (Klass et al., 2018). Several drugs are used for migraine therapy in clinical practice, with different mechanisms that include decreased excitability of cortical circuits, modulation of neuronal plasticity, reduction of circulating levels of calcitonin gene-related peptide (CGRP, a peptide released by nociceptors and implicated in migraine headache) and/or inhibition of cortical spreading depression (Ayata et al., 2006; Costa et al.,

2013; Mantegazza et al., 2010; Sprenger et al., 2018). However, muscarinic agonists are not used in migraine treatment. Our results show that they could be a further option for targeting CSD in the treatment of this debilitating and common disease.

Therapies with muscarinic agonists are often limited by the side effects caused by the incomplete selectivity of these drugs for different muscarinic receptor subtypes and, even more, by their relative central/peripheral effects; although novel compounds are under development that should be more selective and show a better central vs peripheral targeting, which could have a larger clinical use (Bock et al., 2018).

Cholinergic responses in neocortical neurons and their synapses are complex (Munoz and Rudy, 2014). The identification of the detailed muscarinic mechanisms involved in CSD inhibition, which could be multiple and difficult to disentangle, is beyond the scope of this report. Additionally, even a more complete screen of compounds with differential selectivity for receptor subtypes would probably not definitively demonstrate that one and only one subtype is implicated. Our results show that the preferential M1 muscarinic agonist McN-A-343 (although its efficacy at M4 receptors is also high) (Mitchelson, 2012) leads to inhibition of initiation and propagation of CSD in mouse neocortex, inducing an overall decrease of the excitatory/inhibitory ratio. Although we cannot completely exclude that other muscarinic receptors in addition to M1 could be implicated, this action might be targeted in novel pharmacological approaches for the clinical treatment of migraine, in particular with future muscarinic agonists preferentially acting on central receptors, leading to reduced side effects.

Acknowledgements.

This work has been funded by the Investissements d'Avenir-Laboratory of Excellence “Ion Channel Science and Therapeutics” (LabEx ICST ANR-11-LABX-0015-01), France, and by intramural funding from the Foundation IRCCS Istituto Neurologico C.Besta. The laboratory of MM is a member of the “Fédération Hospitalo-Universitaire” InovPain (FHU-InovPain), France.

Credits.

Sarah Zerimech: Conceptualization, Investigation, Formal analysis, Writing - Original Draft, Review & Editing. **Oana Chever:** Conceptualization, Investigation, Formal analysis, Writing - Review & Editing, Supervision. **Paolo Scalmani:** Investigation, Formal analysis. **Lara Pizzamiglio:** Investigation. **Fabrice Duprat:** Software, Writing - Review & Editing. **Massimo Mantegazza:** Conceptualization, Formal analysis, Writing - Original Draft, Review & Editing, Supervision, Project administration, Funding acquisition.

Legends to Figures

Figure 1. Cortical Spreading Depression (CSD) induction with 130mM KCl puffs and propagation in neocortical slices. A. Experimental design for KCl-triggered CSD, ignited by pulse injections (picopump puffs) with increasing volume of 130 mM KCl + 0.1% Fast green (for quantifying the injected area); CSD initiation and propagation were monitored by IOS imaging (light transmittance) and LFP recordings. B. Representative CSD revealed by a negative DC shift in the LFP recordings and changes in IOS at different time points (see methods), scale bar 500 μm . C. Representative images showing a somatosensory neocortical slice (left; Layers 1 to 6 are indicated) and the corresponding IOS image (right) showing the propagation wave front of CSD ignited in that slice by a puff of KCl; the red arrows highlight the different CSD propagation speed across the layers. D. Quantification and comparison of the propagation speed in superficial (1-3) and deeper (4-6) layers (2.98 ± 0.20 mm/min, $n=18$, in L1-3, 2.06 ± 0.10 mm/min, $n=18$, in L4-6; mean \pm SEM); Wilcoxon matched-pairs test, $p < 0.0001$.

Figure 2. Carbachol increases cortical excitability but inhibits CSD. A. Comparisons of LFP recordings in layers 2-3 and 5 of somatosensory cortex slices in control and in presence of carbachol ($100\mu\text{M}$), which induced clear rhythmic oscillatory activities (UP/DOWN states) in layer 5; UP/DOWN states were less evident in layer 3. B. Representative LFP recordings of CSD ignited with a puff of KCl in control (left) and in the presence of carbachol (right); half-width duration (79 ± 12 s mean \pm SEM in control, $n=15$, 69.5 ± 8.5 s with carbachol, $n=12$) and peak amplitude (6.9 ± 0.6 mV mean \pm SEM in control, 7.4 ± 1.6 mV with carbachol) were not modified (Mann Whitney test). C. Scatter plots of CSD threshold of ignition (KCl injection area) which was increased with carbachol ($0.013 \pm 0.057 \text{mm}^2$ in control, $n=18$, $0.025 \pm 0.065 \text{mm}^2$ with carbachol, $n=21$; mean \pm SEM); horizontal bars represent medians (0.013mm^2 in control, 0.025mm^2 with carbachol, Mann Whitney test, $p < 0.0001$); red points are the self-limited CSD events. D. Propagation speed in superficial (left) and deep (right) layers in control and with carbachol, which reduced CSD propagation speed in both superficial layers (2.98 ± 0.20 mm/min in

control, $n=18$, 2.06 ± 0.10 mm/min with carbachol, $n=21$; mean \pm SEM) and deep layers (2.05 ± 0.21 mm/min, $n=18$ in control, 0.91 ± 0.07 mm/min with carbachol, $n=21$; mean \pm SEM); horizontal bars represent medians (L2-3, 2.86 mm/min in control, 2.08 mm/min with carbachol, Mann Whitney test, $p = 0.0009$; L5, 1.87 mm/min in control, 0.88 mm/min with carbachol, Mann Whitney test $p < 0.0001$); red points are the initial speed of the self-limited CSD events.

Figure 3. Carbachol can block CSD propagation. A. representative experiment in which CSD was self-limited and propagated only in a relatively small area around the pipette used for injecting KCl; in particular, it did not propagate to Layer 1 and the pial surface. Scale bar 500 μ m. B. Bar-graph showing that there were no abortive CSD in control (0/44), whereas with carbachol 14% of CSD were abortive (5/35). Fisher's exact test, $p=0.014$.

Figure 4 Involvement of muscarinic receptors on carbachol inhibition of CSD. A. Scatter plots of CSD threshold (area of KCl injection) in control (0.012 ± 0.001 mm² mean \pm SEM; 0.008 mm² median, $n=33$), with carbachol 100 μ M (0.019 ± 0.02 mm², mean \pm SEM, 0.017 mm² median; $n=14$; Kruskal-Wallis test with Dunn post-hoc test, $p=0.022$), carbachol 100 μ M & Atropine 10 μ M (0.011 ± 0.02 mm², mean \pm SEM, 0.009 mm² median; $n=8$), Atropine 10 μ M (0.011 ± 0.001 mm², mean \pm SEM, 0.010 mm² median; $n=9$), or carbachol 100 μ M & telenzepine 100nM (0.007 ± 0.0004 mm² mean \pm SEM; 0.007 mm² median $n=6$). B. upper panel, propagation speed in superficial layers in control (3.23 ± 0.11 mm/min, mean \pm SEM, 3.33 mm/min median; $n=33$), with carbachol 100 μ M (2.26 ± 0.17 mm/min, mean \pm SEM, 2.18 mm/min median; $n=14$; Kruskal-Wallis test with Dunn post-hoc test, $p=0.0004$), carbachol 100 μ M & Atropine 10 μ M (3.00 ± 0.17 mm/min, mean \pm SEM, 3.07 mm/min median; $n=8$), Atropine 10 μ M (3.20 ± 0.22 mm/min, mean \pm SEM, 2.88 mm/min median; $n=9$); or carbachol 100 μ M & telenzepine 100nM (3.47 ± 0.29 mm/min mean \pm SEM; 3.52 mm/min median $n=6$); lower panel, propagation speed in deep layers in control (1.97 ± 0.12 mm/min, mean \pm SEM, 2.05 mm/min median; $n=33$), with carbachol 100 μ M (1.36 ± 0.14 mm/min, mean \pm SEM, 1.37 mm/min median; $n=14$; Kruskal-Wallis test with Dunn post-hoc

test, $p=0.0060$), carbachol $100\mu\text{M}$ & Atropine $10\mu\text{M}$ (1.74 ± 0.16 mm/min, mean \pm SEM, 1.84 mm/min median; $n=8$), Atropine $10\mu\text{M}$ (1.96 ± 0.09 mm/min, mean \pm SEM, 1.90 mm/min median; $n=9$), or carbachol $100\mu\text{M}$ & telenzepine 100nM (2.35 ± 0.27 mm/min mean \pm SEM; 2.28 mm/min median; $n=6$). Horizontal bars represent medians.

Figure 5. Muscarinic activation inhibits CSD initiation and propagation. A. Representative LFP of CSD recorded in control and with the muscarinic agonist McN-A-343 ($30\mu\text{M}$); LFP features were similar in the two conditions: half-length duration was 48 ± 10 s mean \pm SEM, 28 s median, in control ($n=10$), 56 ± 7 s mean \pm SEM, 51 s median, with McN-A-343 ($n=8$); peak amplitude was 5.1 ± 0.5 mV, 5.4mV median, in control, 5.9 ± 0.7 mV, 6.6 mV median, with McN-A-343. B. McN-A-343 increased CSD threshold of ignition ($0.009\pm 0.001\text{mm}^2$ mean \pm SEM, 0.009 mm 2 median, $n=11$, in control; 0.024 ± 0.004 mm 2 mean \pm SEM, 0.027 mm 2 median, with McN-A-343, $n=11$; Mann Whitney test, $p = 0.001$); red points are the self-limited CSD events. C. Reduced CSD propagation speed in superficial layers (3.71 ± 0.25 mm/min, mean \pm SEM, 3.91 mm/min median, in control, $n=11$; 2.37 ± 0.23 mm/min mean \pm SEM, 2.11 mm/min median, with McN-A-343, $n=11$; Mann Whitney test, $p=0.001$) and non-statistically significant trend towards reduction in deep layers (1.61 ± 0.14 mm/min, mean \pm SEM, 1.62 mm/min median, $n=11$, in control; 1.24 ± 0.15 mm/min, mean \pm SEM, 1.16 mm/min median, $n=11$, with McN-A-343; Mann Whitney test, $p=0.13$); red points are the initial speed of the self-limited CSD events. D-E. Further series of experiments in which McN-A-343 ($30\mu\text{M}$) was co-applied with telenzepine (100nM). D. CSD threshold of ignition (Injection area) was similar to the control ($0.089\pm 0.013\text{mm}^2$ mean \pm SEM, 0.084 mm 2 median, $n=7$, in control; $0.074\pm 0.003\text{mm}^2$ mean \pm SEM, 0.075 mm 2 median, $n=6$, with McN-A-343 and telenzepine; Mann Whitney test, $p=0.51$). E. Propagation speed in both superficial layers ($2.92\pm 0.18\text{mm}/\text{min}$, mean \pm SEM, 2.91 mm/min median, $n=7$, in control; $2.90\pm 0.25\text{mm}/\text{min}$, mean \pm SEM, 2.82 mm/min median, $n=6$, with McN-A-343 and telenzepine; Mann Whitney test, $p=0.79$) and deep layers ($1.219\pm 0.15\text{mm}/\text{min}$, mean \pm SEM, 1.24 median mm/min, $n=7$, in control; $1.52\pm 0.18\text{mm}/\text{min}$, mean \pm SEM, 1.59 mm/min median, $n=6$ with carbachol and telenzepine; Mann

Whitney test, $p=0.19$) was not different in comparison with the control condition. Horizontal bars represent medians.

Figure 6. Effect of the muscarinic receptor agonist McN-A-343 on excitatory and inhibitory drive of Layer 2-3 pyramidal neurons. A; Representative traces of spontaneous excitatory post synaptic currents (sEPSCs) recorded from L 2-3 pyramidal neurons in control ($n=6$, above, black) and in presence of McN-A-343 ($30 \mu\text{M}$) ($n=6$, below, violet); scale bars 5pA, 0.5s. B; Cumulative probability plot (left; solid line for control, dashed line for McN-A-343; K-S test, $p<10^{-10}$) and mean values (right; 19.8 ± 0.7 Hz in control, 15.8 ± 0.9 Hz with McN-A-343; t-test, $p=0.0007$) of sEPSCs instantaneous frequency. C; Cumulative probability plot (left; K-S test, $p<10^{-10}$) and mean values (right; 13.3 ± 0.1 pA in control, 17.9 ± 0.2 pA with McN-A-343; t-test, $p<10^{-10}$) of sEPSCs peak amplitude. D; Mean sEPSCs total charge transferred in 103s of recording in control (60 ± 23 pC) and during the perfusion of McN-A-343 (33 ± 19 pC); same recordings as in B and C; Wilcoxon test, $p=0.04$). E; Representative traces of spontaneous excitatory post synaptic currents (sIPSCs) recorded from pyramidal neurons in control ($n=7$, above, black) and in presence of McN-A-343 ($30 \mu\text{M}$) ($n=7$, below, violet); scale bars 7pA, 0.5s. F; Cumulative probability plot (left; K-S test, $p<10^{-10}$) and mean values (right; 2.9 ± 0.1 Hz in control, 7.2 ± 0.2 Hz with McN-A-343; t-test, $p<10^{-10}$) of sIPSCs instantaneous frequency. G; Cumulative probability plot (left; K-S test, $p<10^{-10}$) and mean values (right; right; 26.7 ± 0.7 pA in control, 36.8 ± 0.7 pA with McN-A-343; t-test, $p<10^{-10}$) of sIPSCs peak amplitude. H; Plot of mean sIPSCs total charge transferred in 103s of recording in control (61 ± 22 pC) and during the perfusion of McN-A-343 (247 ± 77 pC); same recordings as in F and G; Wilcoxon test, $p=0.016$.

References

- Ayata, C., Jin, H., Kudo, C., Dalkara, T., Moskowitz, M. A., 2006. Suppression of cortical spreading depression in migraine prophylaxis. *Ann Neurol* 59, 652-661.
- Ayata, C., Lauritzen, M., 2015. Spreading Depression, Spreading Depolarizations, and the Cerebral Vasculature. *Physiol Rev* 95, 953-993.
- Basarsky, T. A., Duffy, S. N., Andrew, R. D., MacVicar, B. A., 1998. Imaging spreading depression and associated intracellular calcium waves in brain slices. *J Neurosci* 18, 7189-7199.
- Becker, K., Eder, M., Ranft, A., von Meyer, L., Zieglgansberger, W., Kochs, E., Dodt, H. U., 2012. Low dose isoflurane exerts opposing effects on neuronal network excitability in neocortex and hippocampus. *PLoS One* 7, e39346.
- Beltramo, R., D'Urso, G., Dal Maschio, M., Farisello, P., Bovetti, S., Clovis, Y., Lassi, G., Tucci, V., De Pietri Tonelli, D., Fellin, T., 2013. Layer-specific excitatory circuits differentially control recurrent network dynamics in the neocortex. *Nat Neurosci* 16, 227-234.
- Bock, A., Schrage, R., Mohr, K., 2018. Allosteric modulators targeting CNS muscarinic receptors. *Neuropharmacology* 136, 427-437.
- Costa, C., Tozzi, A., Rainero, I., Cupini, L. M., Calabresi, P., Ayata, C., Sarchielli, P., 2013. Cortical spreading depression as a target for anti-migraine agents. *J Headache Pain* 14, 62.
- Dreier, J. P., Reiffurth, C., 2015. The stroke-migraine depolarization continuum. *Neuron* 86, 902-922.
- Edelstein, A. D., Tsuchida, M. A., Amodaj, N., Pinkard, H., Vale, R. D., Stuurman, N., 2014. Advanced methods of microscope control using muManager software. *J Biol Methods* 1.
- Francisco, E. D. S., Guedes, R. C. A., 2018. Sub-Convulsing Dose Administration of Pilocarpine Reduces Glycemia, Increases Anxiety-Like Behavior and Decelerates Cortical Spreading Depression in Rats Suckled on Various Litter Sizes. *Front Neurosci* 12, 897.
- Ghoshal, A., Moran, S. P., Dickerson, J. W., Joffe, M. E., Grueter, B. A., Xiang, Z., Lindsley, C. W., Rook, J. M., Conn, P. J., 2017. Role of mGlu5 Receptors and Inhibitory Neurotransmission in M1 Dependent Muscarinic LTD in the Prefrontal Cortex: Implications in Schizophrenia. *ACS Chem Neurosci* 8, 2254-2265.
- Guedes, R. C., Cavalheiro, E. A., 1997. Blockade of spreading depression in chronic epileptic rats: reversion by diazepam. *Epilepsy Res* 27, 33-40.
- Hedrich, U. B., Liautard, C., Kirschenbaum, D., Pofahl, M., Lavigne, J., Liu, Y., Theiss, S., Slotta, J., Escayg, A., Dihne, M., Beck, H., Mantegazza, M., Lerche, H., 2014. Impaired action potential initiation in GABAergic interneurons causes hyperexcitable networks in an epileptic mouse model carrying a human Na(V)1.1 mutation. *J Neurosci* 34, 14874-14889.
- Holthoff, K., Witte, O. W., 1996. Intrinsic optical signals in rat neocortical slices measured with near-infrared dark-field microscopy reveal changes in extracellular space. *J Neurosci* 16, 2740-2749.

- Jo, J., Son, G. H., Winters, B. L., Kim, M. J., Whitcomb, D. J., Dickinson, B. A., Lee, Y. B., Futai, K., Amici, M., Sheng, M., Collingridge, G. L., Cho, K., 2010. Muscarinic receptors induce LTD of NMDAR EPSCs via a mechanism involving hippocalcin, AP2 and PSD-95. *Nat Neurosci* 13, 1216-1224.
- Karatas, H., Erdener, S. E., GURSOY-OZDEMIR, Y., LULE, S., EREN-KOCAK, E., SEN, Z. D., DALKARA, T., 2013. Spreading depression triggers headache by activating neuronal Panx1 channels. *Science* 339, 1092-1095.
- Kirkwood, A., Rozas, C., Kirkwood, J., Perez, F., Bear, M. F., 1999. Modulation of long-term synaptic depression in visual cortex by acetylcholine and norepinephrine. *J Neurosci* 19, 1599-1609.
- Klass, A., Sanchez-Porras, R., Santos, E., 2018. Systematic review of the pharmacological agents that have been tested against spreading depolarizations. *J Cereb Blood Flow Metab* 38, 1149-1179.
- Koga, K., Matsuzaki, Y., Honda, K., Eto, F., Furukawa, T., Migita, K., Irie, K., Mishima, K., Ueno, S., 2017. Activations of muscarinic M1 receptors in the anterior cingulate cortex contribute to the antinociceptive effect via GABAergic transmission. *Mol Pain* 13, 1744806917692330.
- Koroleva, V. I., Bures, J., 1979. Circulation of cortical spreading depression around electrically stimulated areas and epileptic foci in the neocortex of rats. *Brain Res* 173, 209-215.
- Koroleva, V. I., Bures, J., 1980. Blockade of cortical spreading depression in electrically and chemically stimulated areas of cerebral cortex in rats. *Electroencephalogr Clin Neurophysiol* 48, 1-15.
- Kurowski, P., Gawlak, M., Szulczyk, P., 2015. Muscarinic receptor control of pyramidal neuron membrane potential in the medial prefrontal cortex (mPFC) in rats. *Neuroscience* 303, 474-488.
- Lauritzen, M., 1994. Pathophysiology of the migraine aura. The spreading depression theory. *Brain* 117 (Pt 1), 199-210.
- Leao, A. A., 1947. Further observations on the spreading depression of activity in the cerebral cortex. *J Neurophysiol* 10, 409-414.
- Lebois, E. P., Thorn, C., Edgerton, J. R., Popiolek, M., Xi, S., 2018. Muscarinic receptor subtype distribution in the central nervous system and relevance to aging and Alzheimer's disease. *Neuropharmacology* 136, 362-373.
- Li, Z., Prus, A. J., Dai, J., Meltzer, H. Y., 2009. Differential effects of M1 and 5-hydroxytryptamine1A receptors on atypical antipsychotic drug-induced dopamine efflux in the medial prefrontal cortex. *J Pharmacol Exp Ther* 330, 948-955.
- Liautard, C., Scalmani, P., Carriero, G., de Curtis, M., Franceschetti, S., Mantegazza, M., 2013. Hippocampal hyperexcitability and specific epileptiform activity in a mouse model of Dravet syndrome. *Epilepsia* 54, 1251-1261.
- Lorincz, M. L., Gunner, D., Bao, Y., Connelly, W. M., Isaac, J. T., Hughes, S. W., Crunelli, V., 2015. A distinct class of slow (~0.2-2 Hz) intrinsically bursting layer 5 pyramidal neurons determines UP/DOWN state dynamics in the neocortex. *J Neurosci* 35, 5442-5458.
- Mantegazza, M., Cestele, S., 2018. Pathophysiological mechanisms of migraine and epilepsy: Similarities and differences. *Neurosci Lett* 667, 92-102.

- Mantegazza, M., Curia, G., Biagini, G., Ragsdale, D. S., Avoli, M., 2010. Voltage-gated sodium channels as therapeutic targets in epilepsy and other neurological disorders. *Lancet Neurol* 9, 413-424.
- Mitchelson, F. J., 2012. The pharmacology of McN-A-343. *Pharmacol Ther* 135, 216-245.
- Munoz, W., Rudy, B., 2014. Spatiotemporal specificity in cholinergic control of neocortical function. *Curr Opin Neurobiol* 26, 149-160.
- Pietrobon, D., Moskowitz, M. A., 2013. Pathophysiology of migraine. *Annu Rev Physiol* 75, 365-391.
- Pietrobon, D., Moskowitz, M. A., 2014. Chaos and commotion in the wake of cortical spreading depression and spreading depolarizations. *Nat Rev Neurosci* 15, 379-393.
- Poorthuis, R. B., Enke, L., Letzkus, J. J., 2014. Cholinergic circuit modulation through differential recruitment of neocortical interneuron types during behaviour. *J Physiol* 592, 4155-4164.
- Pronin, A. N., Wang, Q., Slepak, V. Z., 2017. Teaching an Old Drug New Tricks: Agonism, Antagonism, and Biased Signaling of Pilocarpine through M3 Muscarinic Acetylcholine Receptor. *Mol Pharmacol* 92, 601-612.
- Sanchez-Vives, M. V., McCormick, D. A., 2000. Cellular and network mechanisms of rhythmic recurrent activity in neocortex. *Nat Neurosci* 3, 1027-1034.
- Schindelin, J., Rueden, C. T., Hiner, M. C., Eliceiri, K. W., 2015. The ImageJ ecosystem: An open platform for biomedical image analysis. *Mol Reprod Dev* 82, 518-529.
- Schytz, H. W., Wienecke, T., Olesen, J., Ashina, M., 2010. Carbachol induces headache, but not migraine-like attacks, in patients with migraine without aura. *Cephalalgia* 30, 337-345.
- Schytz, H. W., Wienecke, T., Oturai, P. S., Olesen, J., Ashina, M., 2009. The cholinomimetic agent carbachol induces headache in healthy subjects. *Cephalalgia* 29, 258-268.
- Sprenger, T., Viana, M., Tassorelli, C., 2018. Current Prophylactic Medications for Migraine and Their Potential Mechanisms of Action. *Neurotherapeutics* 15, 313-323.
- Tang, Y. T., Mendez, J. M., Theriot, J. J., Sawant, P. M., Lopez-Valdes, H. E., Ju, Y. S., Brennan, K. C., 2014. Minimum conditions for the induction of cortical spreading depression in brain slices. *J Neurophysiol* 112, 2572-2579.
- Thorn, C. A., Popiolek, M., Stark, E., Edgeron, J. R., 2017. Effects of M1 and M4 activation on excitatory synaptic transmission in CA1. *Hippocampus* 27, 794-810.
- Tottene, A., Conti, R., Fabbro, A., Vecchia, D., Shapovalova, M., Santello, M., van den Maagdenberg, A. M., Ferrari, M. D., Pietrobon, D., 2009. Enhanced excitatory transmission at cortical synapses as the basis for facilitated spreading depression in Ca(v)2.1 knockin migraine mice. *Neuron* 61, 762-773.
- Vinogradova, L. V., 2018. Initiation of spreading depression by synaptic and network hyperactivity: Insights into trigger mechanisms of migraine aura. *Cephalalgia* 38, 1177-1187.
- Voss, L. J., Garcia, P. S., Hentschke, H., Banks, M. I., 2019. Understanding the Effects of General Anesthetics on Cortical Network Activity Using Ex Vivo Preparations. *Anesthesiology* 130, 1049-1063.

Wester, J. C., Contreras, D., 2013. Differential modulation of spontaneous and evoked thalamocortical network activity by acetylcholine level in vitro. *J Neurosci* 33, 17951-17966.

Williams, S. R., Fletcher, L. N., 2019. A Dendritic Substrate for the Cholinergic Control of Neocortical Output Neurons. *Neuron* 101, 486-499 e484.

Figure 1
[Click here to download high resolution image](#)

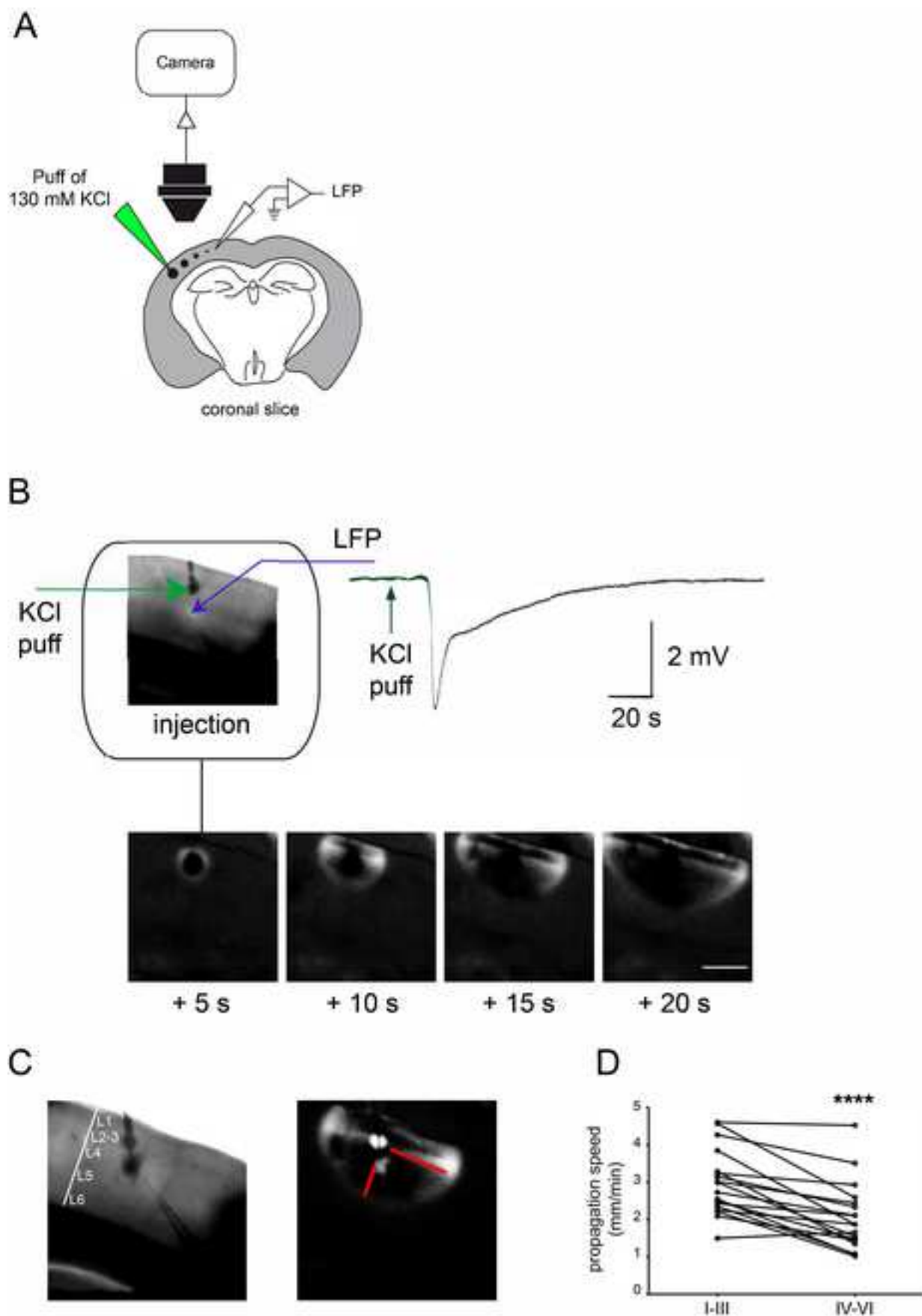


Figure 3
[Click here to download high resolution image](#)

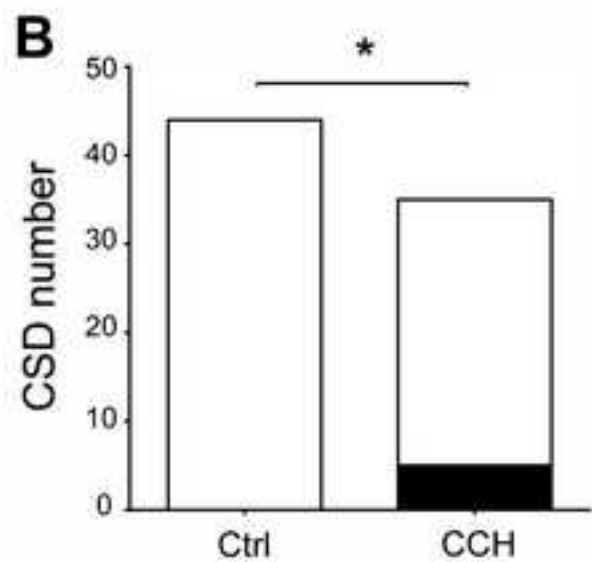
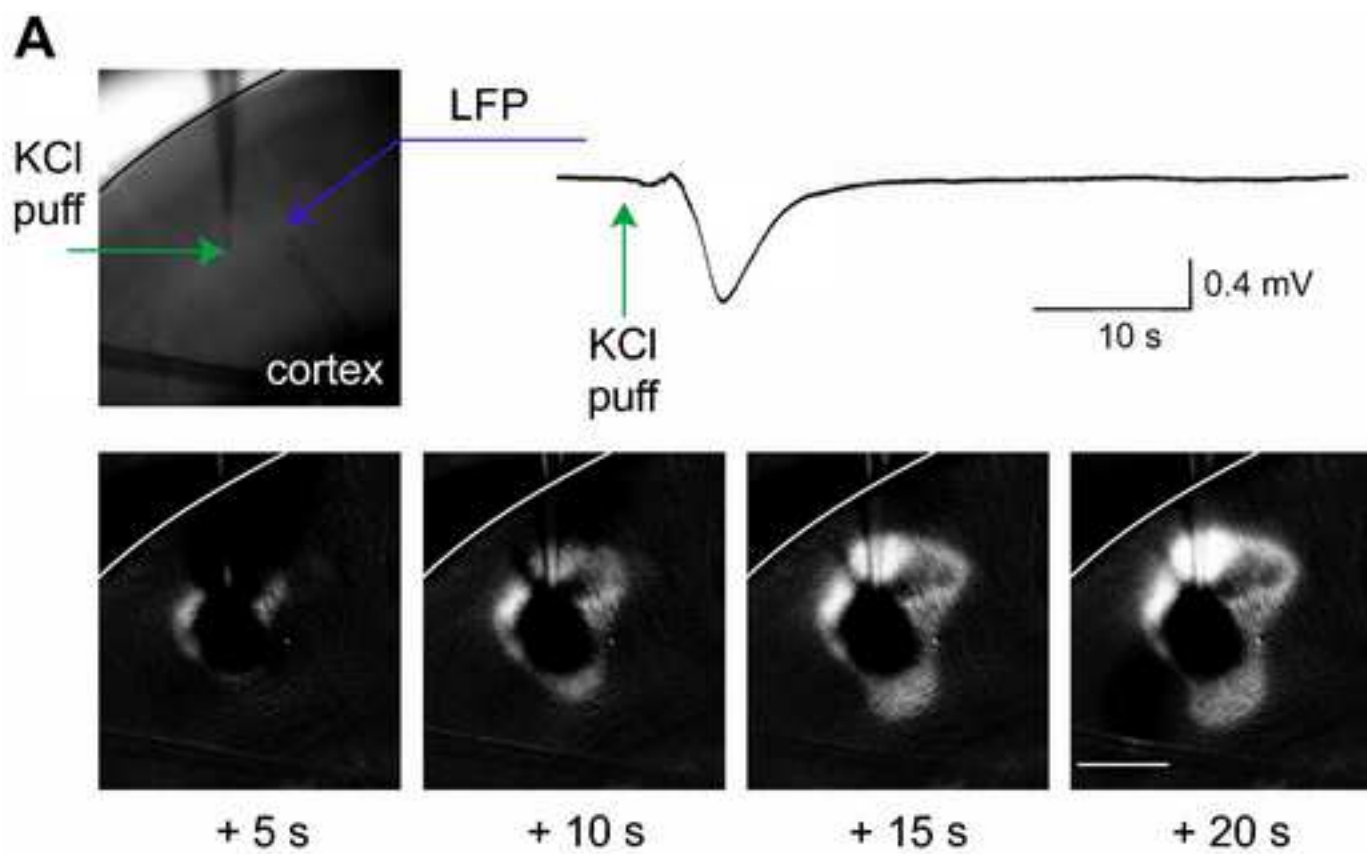


Figure 4
[Click here to download high resolution image](#)

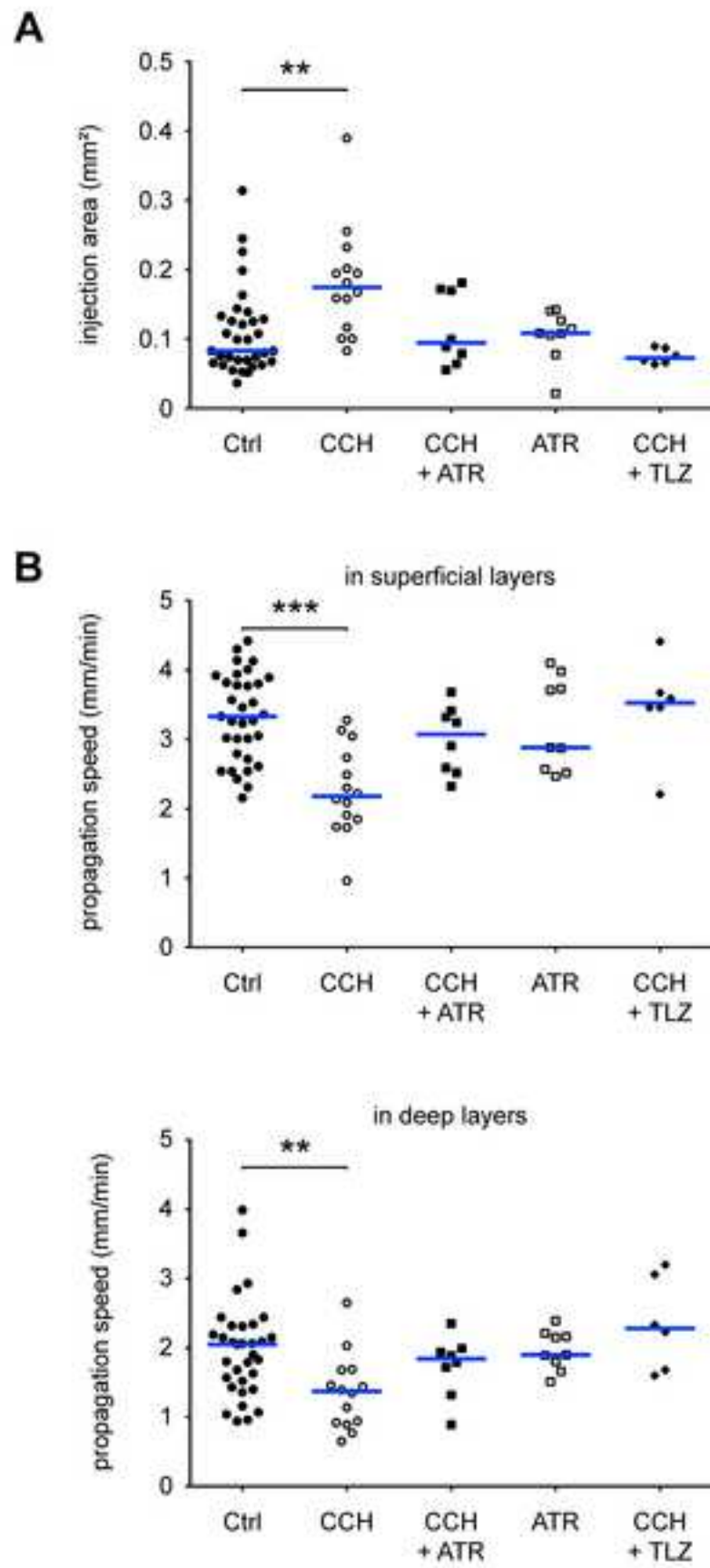
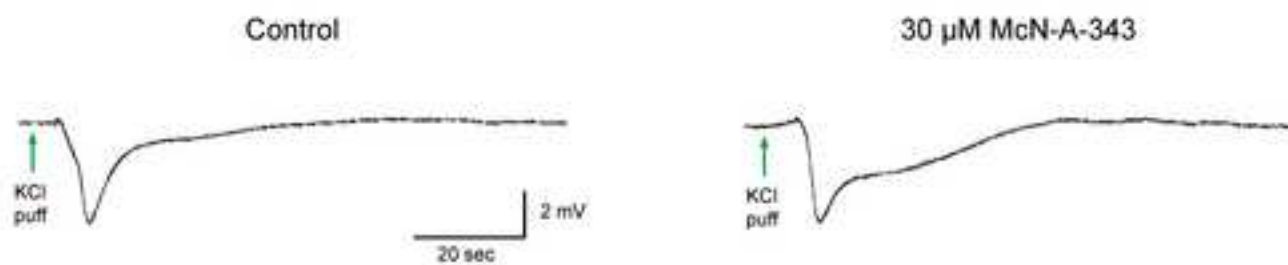
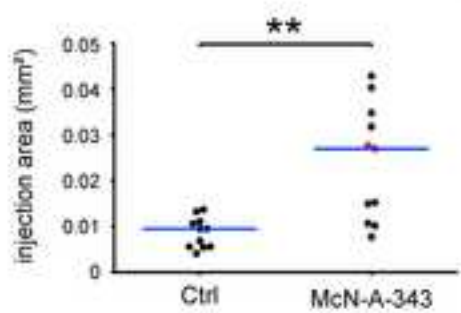


Figure 5
[Click here to download high resolution image](#)

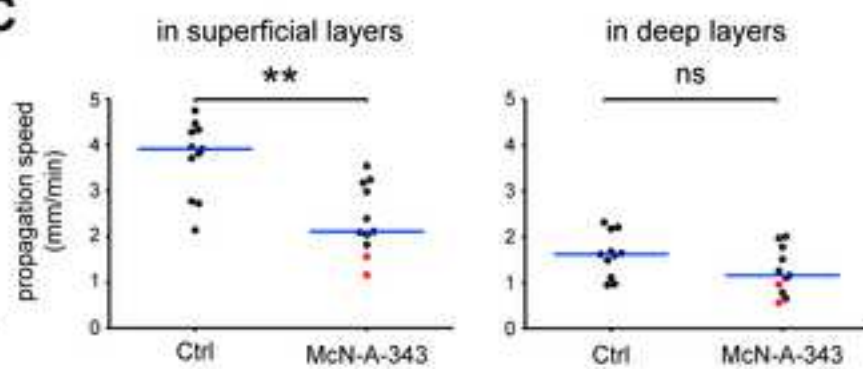
A



B



C



D

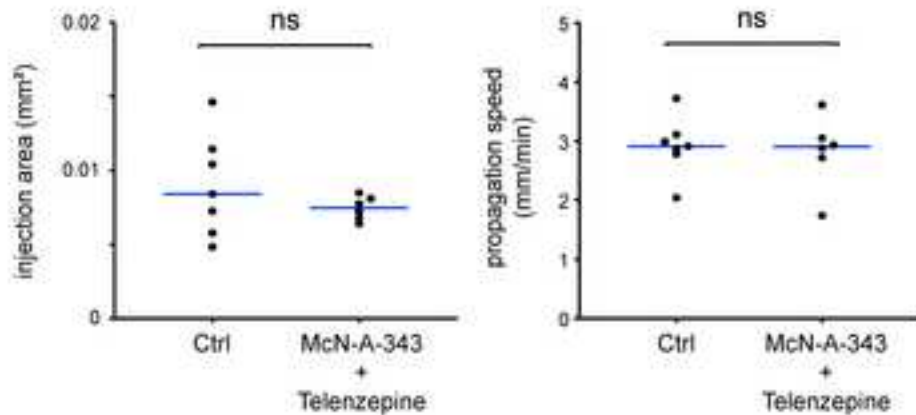
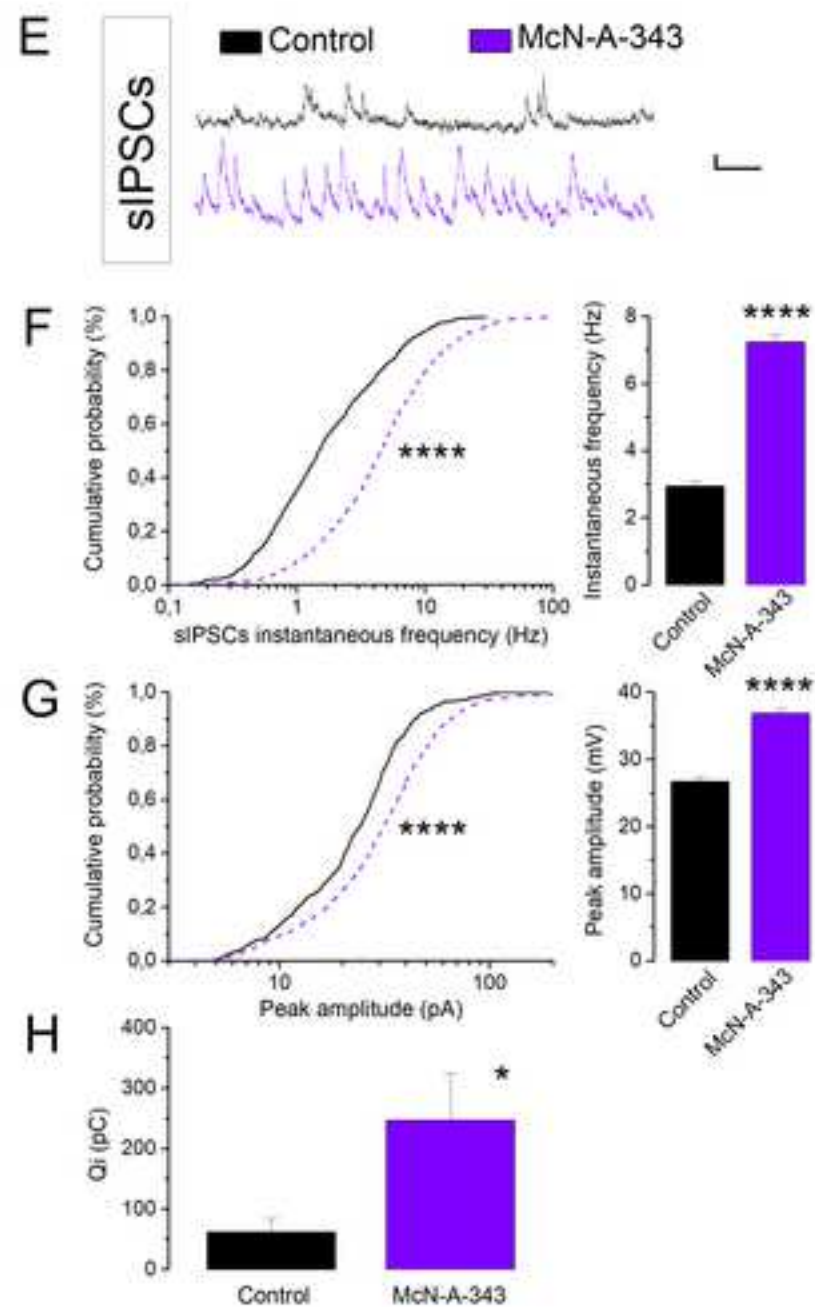
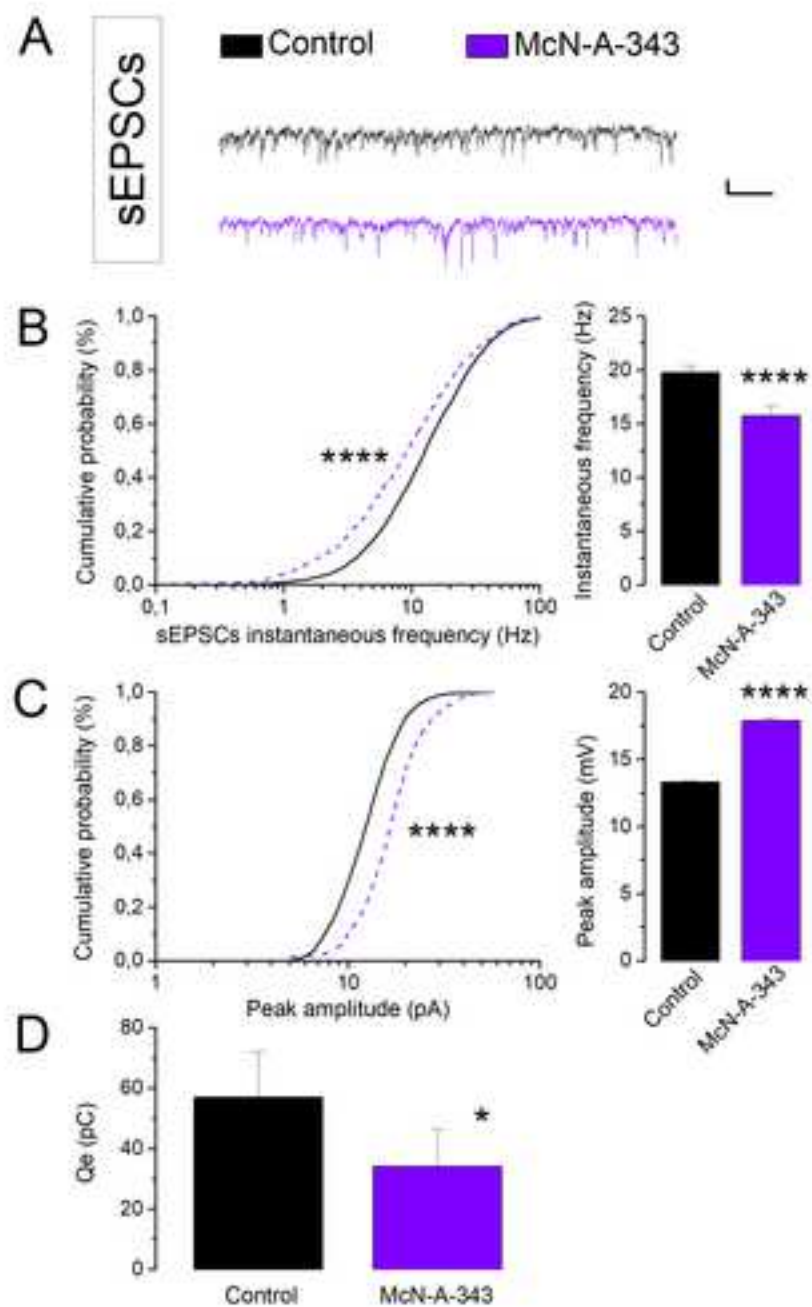


Figure 6
[Click here to download high resolution image](#)



Video 1 Control CSD

[Click here to download Supplementary Material: Supplementary Video 1.mp4](#)

Video 2 Self limited CSD with carbachol

[Click here to download Supplementary Material: Supplementary Video 2.mp4](#)